International Forum on Aeroelasticity and Structural Dynamics
IFASD 2024
17 – 21 June 2024, The Hague, The Netherlands

INCLUDING GRADIENT-BASED TRANSIENT GUST OPTIMIZATION IN ASTROS

Joshua Deslich[1], Doug Neill[2], Kevin McHugh[1], and Raymond Kolonay[1]

[1]U.S. Air Force Research Laboratory, Wright-Patterson Air Force Base, Ohio, USA
joshua.deslich.1@us.af.mil, kevin.mchugh.3@us.af.mil, raymond.kolonay@us.af.mil

[2]ICME Design, Computational Engineering Software LLC., San Antonio, Texas, USA
doug.neill@icmedesign.com

Historically gust loads have been excluded from early stages in the aircraft design process in part due to their computational complexity. As air vehicles push the envelops of aspect ratio, there is an increasing need to understand the implications of gust loads as well as incorporating them in the early design process. Work was performed using ASTROS and OpenMDAO to include aeroelastic gust analysis for gust-based stress constraints as well as formalization of the sensitivity equations for the aeroelastic gust responses. The initial implementation of the stress-based gust optimization shows favorable behavior for simple design problems and builds confidence in the ability to increase complexity in later development efforts. Results for both analytical stress sensitivity and finite difference approximation optimization problems are discussed as well as the behavior of the constraint space for larger scale design problems.

1 TECHNICAL BACKGROUND

Recent advancements in conceptual and preliminary air vehicle design seek to inject higher-fidelity analyses into early design processes to capture physics-based aircraft performance as soon as possible in the design cycle. This philosophy is often realized in the form of high-fidelity coupled aeroelastic or aeroservoelastic design via analysis including quasi-steady maneuver loads or flutter [1]. However, there are relatively few efforts to include transient aeroelastic solutions in design, and those cases are limited in the context of a conceptual design process [2–4]. This work seeks to leverage an existing aeroelastic solver, ASTROS, and enhance the design capability to include analytical stress gradients for designing a high aspect ratio wing under transient gust stress constraints.

Previous development of ASTROS has excluded transient gusts from optimization due to computational cost and was primarily used for checking final designs [5]. Including gust analysis in the early stages of aeroelastic conceptual design could mitigate late-stage redesigns to account for gust loads certification [6, 7]. Current work performed at NASA is targeting gust constraints via root-bending moment constraints with high-fidelity aeroelastic solutions [4]. As the aspect ratio of the configurations of interest increases so does the need for consideration of gust responses in the early design process as well as consideration for non-linear aeroelastic effects.

2 DEVELOPMENT OF GUST SENSITIVITY EQUATIONS

The gust response of a flexible wing in the frequency domain is a straightforward computation which uses the aeroelastic equations of motion and an aerodynamic gust load to solve for the displacements as a function of frequency. The left-hand side of Equation 1 contains the aeroelastic equations of motion and the right-hand side contains a load vector which represents the aerodynamic gust load as a function of analysis frequency.

Distribution Statement A: Approved for Public Release; Distribution is Unlimited. PA# AFRL-2024-2907.

$$\left[-\omega_a^2\mathbf{M} + i\omega_a\left[\mathbf{B} - \frac{qb}{2v}\mathbf{A}^I(\omega_a)\right] + \mathbf{K} - \frac{q}{k}\mathbf{A}^R(\omega_a)\right]\{\mathbf{u}\} = \left\{P_h^f(\omega_a)\right\} \tag{1}$$

Equation 1 is solved in modal coordinates, which requires generalized mass, stiffness, damping, and aerodynamic matrices. Since the gust response is calculated at a single Mach number and over a range of prescribed frequencies, the unsteady aerodynamics are computed at each analysis frequency and then used to directly solve the equations of motion. This method is similar to other dynamic solutions, such as flutter, in which ASTROS and NASTRAN construct interpolant models of the aerodynamics over a range of Mach numbers and reduced frequencies. The computational cost and memory usage directly scales with the number of frequencies which are included in the analysis.

Unlike a P-K flutter solve, gust displacements are directly solved at the analysis frequency and the engineer is responsible for describing the gust load of interest as a function of frequency. A convenient form of a general dynamic gust force is shown in Equation 2:

$$P_h^f = qw_g P_w P_\delta \tag{2}$$

Where q is the dynamic pressure and w_g is the 'gust scale factor'. Equation 2 comprises of the gust shaped described by P_w, which is defined by the engineer, and the aerodynamic gust force, P_δ, which is the unsteady aerodynamic gust load. Equation 3 contains Q_{hj} which are the unsteady gust loads on a rigid aircraft and a sinusoidal function which relates the downwash at each analysis frequency to the unsteady gust loads [5].

$$P_\delta = Q_{hj}cos(\gamma_j)e^{-i\omega_a(x_j - x_0)/V} \tag{3}$$

With all components of the gust aeroelastic equation of motion defined, the derivative of the displacements with respect to a design variable, in this case property thickness, is computed:

$$\begin{aligned}\frac{\partial\, {}^{m\,\mathrm{x}\,t}\mathbf{u}}{\partial x_i} = \left[-\omega_a^2\, {}^{m\,\mathrm{x}\,m}\mathbf{M} + i\omega_a\left[{}^{m\,\mathrm{x}\,m}\mathbf{B} + \frac{qb}{2v}\,{}^{m\,\mathrm{x}\,m}\mathbf{A}^I(k_a)\right] + {}^{m\,\mathrm{x}\,m}\mathbf{K} - q\,{}^{m\,\mathrm{x}\,m}\mathbf{A}^R(k_a)\right]^{-1} \ldots \\ \left[\frac{\partial\, {}^{m\,\mathrm{x}\,t}P_h^f}{\partial x_i} - \left(-\omega_a^2\frac{\partial\, {}^{m\,\mathrm{x}\,m}\mathbf{M}}{\partial x_i} + i\omega_a\left[\frac{\partial\, {}^{m\,\mathrm{x}\,m}\mathbf{B}}{\partial x_i} + \frac{qb}{2v}\frac{\partial\, {}^{m\,\mathrm{x}\,m}\mathbf{A}^I(k_a)}{\partial x_i}\right] + \frac{\partial\, {}^{m\,\mathrm{x}\,m}\mathbf{K}}{\partial x_i} - q\frac{\partial\, {}^{m\,\mathrm{x}\,m}\mathbf{A}^R(k_a)}{\partial x_i}\right) {}^{m\,\mathrm{x}\,t}\{\mathbf{u}\}\right]\end{aligned} \tag{4}$$

Where $k_a = \frac{\omega_a b}{V}$, m is the number of structural mode shapes and t is the number of analysis frequencies. The partial derivative of the structural mass, damping, and stiffness equations is generally described by Equation 5:

$$\frac{\partial\mathbf{M}}{\partial x_i} = \frac{\partial\phi^T}{\partial x_i}M\phi + \phi^T\frac{\partial M}{\partial x_i}\phi + \phi^T M\frac{\partial\phi}{\partial x_i} \tag{5}$$

Distribution Statement A: Approved for Public Release; Distribution is Unlimited. PA# AFRL-2024-2907.

For this work, and generally within linear aeroelastic solvers, it is assumed that the mode shapes remain constant about a design point. In the context of optimization, the design point is updated each iteration, which will update the mode shapes and structural frequencies, but for the expansion about a fixed design point and subsequent search direction calculation, the mode shapes and structural frequencies are fixed. Additionally it is assumed that structural damping is including via modal damping which is defined by the engineer, typically 3% and is linked to the structural natural frequencies. Generally Equation 5 reduces to:

$$\frac{\partial \mathbf{M}}{\partial x_i} = \phi^T \frac{\partial M}{\partial x_i} \phi \tag{6}$$

Unlike steady aerodynamics or flutter analysis, there are two components to the aerodynamics for gust analysis. These two components are the two-way coupled aerodynamic-structures interaction, $\mathbf{Q}_{hh}(k)$, and the gust force which is a one-way aerodynamic on structures interaction, $\mathbf{Q}_{hj}(k)$. For the two-way coupled aerodynamics, the generalized aerodynamics is expressed as:

$$\mathbf{Q}_{hh}(\omega_s, \omega_{hp}, M) = \phi^T(\omega_s) \cdot UG^T \cdot S \cdot A^{-1}(\omega_{hp}, M) \cdot D \cdot UG \cdot \phi(\omega_s) \tag{7}$$

Differentiating Equation 7 with respect to a thickness design variable yields:

$$\begin{aligned}
\frac{\partial \mathbf{Q}(\omega_s, \omega_{hp}, M)}{\partial x_i} = &\frac{\partial \phi^T(\omega_s)}{\partial x_i} \left(UG^T \cdot S \cdot A^{-1}(\omega_{hp}, M) \cdot D \cdot UG \cdot \phi(\omega_s) \right) + ... \\
&\frac{\partial UG^T}{\partial x_i} \left(\phi^T(\omega_s) \cdot S \cdot A^{-1}(\omega_{hp}, M) \cdot D \cdot UG \cdot \phi(\omega_s) \right) + ... \\
&\frac{\partial S}{\partial x_i} \left(\phi^T(\omega_s) \cdot UG^T \cdot A^{-1}(\omega_{hp}, M) \cdot D \cdot UG \cdot \phi(\omega_s) \right) + ... \\
&\frac{\partial A^{-1}(\omega_{hp}, M)}{\partial x_i} \left(\phi^T(\omega_s) \cdot S \cdot UG^T \cdot D \cdot UG \cdot \phi(\omega_s) \right) + ... \\
&\frac{\partial D}{\partial x_i} \left(\phi^T(\omega_s) \cdot UG^T \cdot S \cdot A^{-1}(\omega_{hp}, M) \cdot UG \cdot \phi(\omega_s) \right) + ... \\
&\frac{\partial UG}{\partial x_i} \left(\phi^T(\omega_s) \cdot UG^T \cdot S \cdot A^{-1}(\omega_{hp}, M) \cdot \phi(\omega_s) \right) + ... \\
&\frac{\partial \phi(\omega_s)}{\partial x_i} \left(\phi^T(\omega_s) \cdot UG^T \cdot S \cdot A^{-1}(\omega_{hp}, M) \cdot D \cdot UG \cdot \phi(\omega_s) \right)
\end{aligned} \tag{8}$$

Equation 8 contains many terms which are invariant for a given design sensitivity. Any term which is a function of structural frequency, ω_s, is invariant as well as any term which is a function for reduced frequency hard-points w_{hp}. Additionally, the spline and integration matrices UG, D and S are dependent only on the aerodynamic mesh points and structural mesh points, making them invariant to the changes in thickness. This reduces Equation 8 to:

$$\begin{aligned}
\frac{\partial \mathbf{Q}(\omega_s, \omega_{hp}, k_a, M)}{\partial x_i} = &\frac{\partial \phi^T(\omega_s)}{\partial x_i} \left(UG^T \cdot S \cdot A^{-1}(\omega_{hp}, M) \cdot D \cdot UG \cdot \phi \right) + ... \\
&\frac{\partial \phi}{\partial x_i} \left(\phi^T(\omega_s) \cdot UG^T \cdot S \cdot A^{-1}(\omega_{hp}, M) \cdot D \cdot UG \cdot \phi \right)
\end{aligned} \tag{9}$$

Distribution Statement A: Approved for Public Release; Distribution is Unlimited. PA# AFRL-2024-2907.

In this work it is assumed that the mode shapes, ϕ, are held constant about a design point, which makes them invariant to perturbations in thickness, further reducing Equation 9 to a constant. Likewise the one-way coupled aerodynamics is represented by:

$$\mathbf{Q}_{hj}(\omega_s, \omega_{hp}, M) = \phi^T(\omega_s) \cdot UG^T \cdot S \cdot A^{-1}(\omega_{hp}, M) \tag{10}$$

Like Equation 8, the derivative of Equation 10 with respect to a thickness design variable is a constant. All of this shows that the unsteady aerodynamics are constant for a given design point and set of reduced frequency hard-points, but ASTROS and other linear aeroelastic solvers employ interpolant functions to approximate the unsteady aerodynamics over a continuous range of reduced frequencies. In this case, ASTROS uses a cubic interpolation function for the unsteady aerodynamics of both the two-way coupled and one-way coupled aerodynamics. Using Equations 11 - 14, the unsteady aerodynamics are approximated for any reduced frequency within the bounds of the specified reduced frequency hard points.

$$G_{ij} = \begin{cases} 0 & \text{for } i = j = nhdpts + 1 \\ 1 & \text{for } i = nhdpts + 1 \text{ or } j = nhdpts + 1 \\ \|k_i - k_j\|^3 + \|k_i + k_j\|^3 & \text{for } i \text{ or } j \leq nhdpts \end{cases} \tag{11}$$

$$p_{aj} = \begin{cases} 0 & \text{for } j = nhdpts + 1 \\ \|k_a - k_j\|^3 + \|k_a + k_j\|^3 & \text{for } j \leq nhdpts \end{cases} \tag{12}$$

$$C_j = G_{ij}^{-1} p_{vj} \tag{13}$$

$$\mathbf{A}_{hh}\left(k_a\right) = \sum_{j=1}^{nhpts} C_j \left[Q_{hh}^R(k_j) + \frac{i}{k_j} Q_{hh}^I(k_j) \right] \tag{14}$$

For flutter sensitivity analysis there is a sensitivity of $\mathbf{A}_{hh}$ to changes in k_a since the flutter solution is sensitive to changes in aerodynamic damping. In the case of gust analysis, the k_a are the specified analysis frequencies which do not change in the design problem. For flutter sensitivity analysis, it is noted that aerodynamic sensitivities are incorporated through the chain-rule:

$$\frac{\partial \mathbf{A}_{hh}}{\partial x_i} = \frac{\partial \mathbf{A}_{hh}}{\partial k} \frac{\partial k}{\partial x_i} \tag{15}$$

However, the reduced frequencies used in the flutter sensitivity calculation are the structural reduced frequencies. In the case of gust analysis it is assumed that the reduced frequencies used in the analysis of the unsteady aerodynamics are constant and is independent of changes in the structural reduced frequencies. The resulting equation for displacement sensitivities becomes:

Distribution Statement A: Approved for Public Release; Distribution is Unlimited. PA# AFRL-2024-2907.

$$\frac{\partial \overset{m \text{ x } t}{\mathbf{u}}}{\partial x_i} = \left[-\omega_a^2 \overset{m \text{ x } m}{\mathbf{M}} + i\omega_a \overset{m \text{ x } m}{\mathbf{B}} + \overset{m \text{ x } m}{\mathbf{K}}\right]^{-1} \ldots \left[-\left(-\omega_a^2 \frac{\partial \overset{m \text{ x } m}{\mathbf{M}}}{\partial x_i} + i\omega_a \frac{\partial \overset{m \text{ x } m}{\mathbf{B}}}{\partial x_i} + \frac{\partial \overset{m \text{ x } m}{\mathbf{K}}}{\partial x_i}\right) \overset{m \text{ x } t}{\{\mathbf{u}\}}\right] \tag{16}$$

While the displacement sensitivities are an important building block for aeroelastic optimization problems, engineers are typically concerned with failure criteria, in this case the limit loads of a structure. These limits can be expressed with Von Mises stress constraints, expressed by:

$$g = \left[\left(\frac{\sigma_x}{\sigma_{x_{lim}}}\right)^2 + \left(\frac{\sigma_y}{\sigma_{y_{lim}}}\right)^2 - \left(\frac{\sigma_x \sigma_y}{\sigma_{x_{lim}} \sigma_{y_{lim}}}\right) + \left(\frac{\tau_{xy}}{\tau_{xy_{lim}}}\right)^2\right]^{\frac{1}{2}} - 1 \tag{17}$$

In this case, the normal stress are used and can be recovered using the stress recovery matrix S and the g-set displacements u_g.

$$\sigma = \begin{Bmatrix} \sigma_x \\ \sigma_y \\ \tau_{xy} \end{Bmatrix} = S^T u_g \tag{18}$$

Within ASTROS, the Von Mises stress sensitivities are computed using the direct method:

$$\frac{\partial g}{\partial x_i} = \frac{\partial f}{\partial x_i} + \frac{\partial f}{\partial u_g}^T \frac{\partial u_g}{\partial x_i} \tag{19}$$

From Equation 19, there are two unknown terms, $\frac{\partial f}{\partial x_i}$ and $\frac{\partial f}{\partial u_g}^T$ while $\frac{\partial u_g}{\partial x_i}$ has previously been computed. $\frac{\partial f}{\partial u_g}$ derived from Equation 17 yielding:

$$\frac{\partial f^T}{\partial u_g} = \frac{1}{2(g+1)} \left[\left(\frac{2\sigma_x}{\sigma_{x_{lim}}^2} - \frac{\sigma_y}{\sigma_{x_{lim}} \sigma_{y_{lim}}}\right) \frac{\partial \sigma_x}{\partial u_g} + \ldots \left(\frac{2\sigma_y}{\sigma_{y_{lim}}^2} - \frac{\sigma_x}{\sigma_{x_{lim}} \sigma_{y_{lim}}}\right) \frac{\partial \sigma_y}{\partial u_g} + \frac{2\tau_{xy}}{\tau_{xy_{lim}}^2} \frac{\partial \tau_{xy}}{\partial u_g}\right] \tag{20}$$

$$\frac{\partial \sigma}{\partial u_g} = S^T \tag{21}$$

Similarly, the $\frac{\partial f}{\partial x_i}$ term is derived:

Distribution Statement A: Approved for Public Release; Distribution is Unlimited. PA# AFRL-2024-2907.

$$\frac{\partial f}{\partial x_i}^{1\,\mathrm{x}\,t} = \frac{1}{2(g+1)}^{1\,\mathrm{x}\,t} \left[\left(\frac{2\sigma_x}{\sigma_{x_{lim}}^2}^{t\,\mathrm{x}\,1} - \frac{\sigma_y}{\sigma_{x_{lim}}\sigma_{y_{lim}}}^{t\,\mathrm{x}\,1} \right) \frac{\partial S_x}{\partial x_i}^{1\,\mathrm{x}\,n}{}^{n\,\mathrm{x}\,t} u_g + \ldots \right.$$
$$\left. \left(\frac{2\sigma_y}{\sigma_{y_{lim}}^2}^{1\,\mathrm{x}\,t} - \frac{\sigma_x}{\sigma_{x_{lim}}\sigma_{y_{lim}}}^{1\,\mathrm{x}\,t} \right) \frac{\partial S_y}{\partial x_i}^{1\,\mathrm{x}\,n}{}^{n\,\mathrm{x}\,t} u_g + \frac{2\tau_{xy}}{\tau_{xy_{lim}}^2}^{1\,\mathrm{x}\,t} \frac{\partial S_{xy}}{\partial x_i}^{1\,\mathrm{x}\,n}{}^{n\,\mathrm{x}\,t} u_g \right] \tag{22}$$

Like $\frac{\partial \sigma}{\partial u_g}$, ASTROS returns $\frac{\partial S}{\partial x_i}$ used in Equation 22 and is computed via finite difference within ASTROS.

3 AEROELASTIC MODEL

The aeroelastic model in this study is a simple cantilevered plate shown in Figure 1. The structural model, in black, has a span of 120.0 inches and a chord of 42.0 while the aerodynamic model, in blue, has a span of 120.0 inches and a chord of 48.0 inches. The aerodynamic model contains 25 aerodynamic panels with equal spacing and are splined to the structure with an infinite plate spline. For this study, linear quadratic shell elements are used to represent the structure. The panel is designed using 6061-T6 Aluminum properties and the yield stresses in tension, compression, and shear are set to 25000 psi. A small amount of structural damping, 3%, is included in the model to allow the response to exhibit 'ring-down' behavior and dampen the aeroelastic reponse.

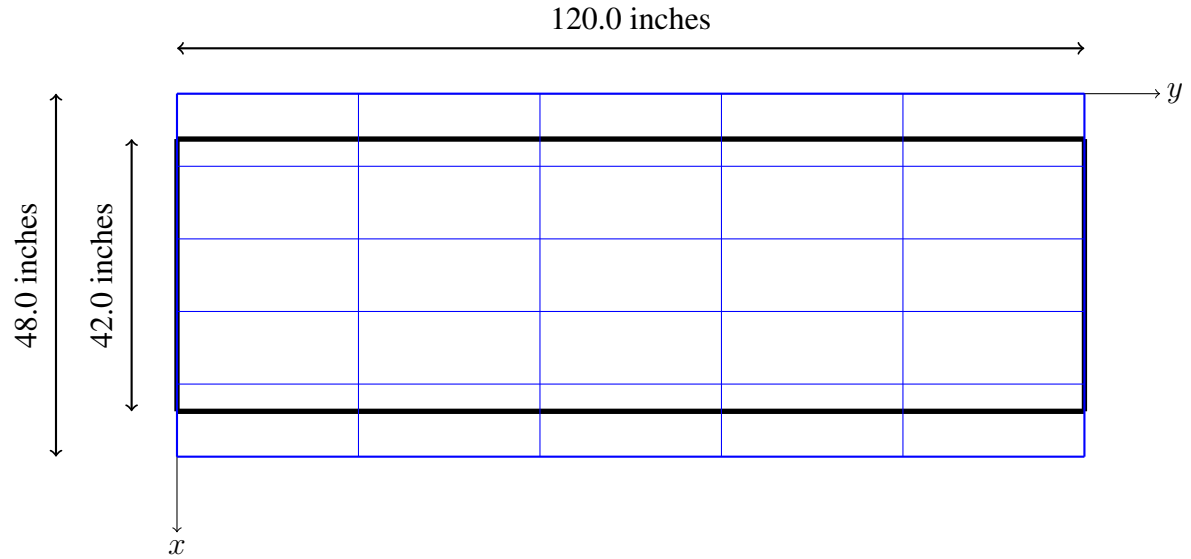

Figure 1: Plate wing model with structural layout in black and the aerodynamic model shown in blue.

Distribution Statement A: Approved for Public Release; Distribution is Unlimited. PA# AFRL-2024-2907.

4 OPTIMIZATION RESULTS

A simple optimization problem was formulated to understand the implications of implementing stress constraints for gusts. Equation 23 shows the simple problem whose goal is to minimize the weight of the panel by varying the panel thickness subject to Von Mises stress constraints. Two optimization studies were conducted for this problem, one using the analytical sensitivity formulation in Equation 19 and the other using a total finite difference for the stress constraints.

$$\begin{aligned} &\text{minimize} && mass \\ &\text{w.r.t} && thickness \\ &\text{subject to} && \sigma(t_i)_{vm} < 0.0 \end{aligned} \tag{23}$$

For this work, OpenMDAO was used to construct the optimization problem with a SLSQP optimization algorithm [8]. The current capabilities of ASTROS make it difficult to implement new analysis types within an optimization and is left up to future development work. A fixed gust load was selected for the design problem with increased magnitude near the structural frequencies of interest. Over the remaining frequency range, the magnitude of the gust load is set to be zero. The initial design point is set for a 6 inch panel, with Figure 2 showing the modal displacement response, with maximum magnitude corresponding to a harmonic response of the structural modes. The bending mode of the 6 inch panel has a natural frequency of 9.15 Hz, which corresponds to the maximum modal response of the mode and near the torsion mode with a 40.24 Hz natural frequency there is a slight increase in amplitude.

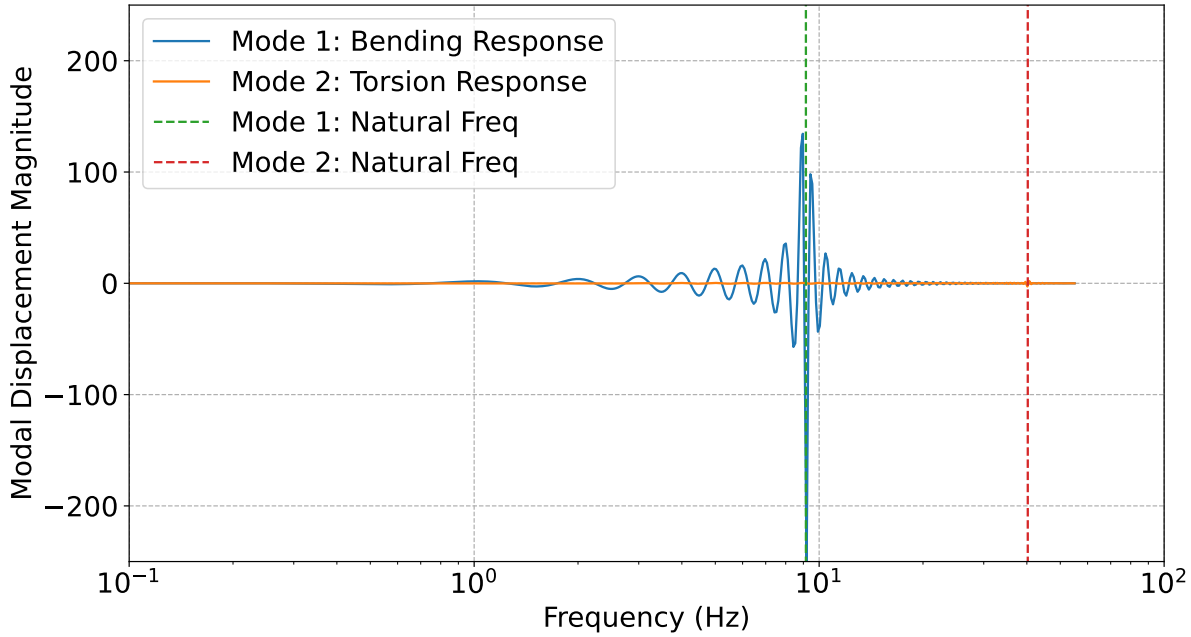

Figure 2: Modal Response of a Panel Wing Configuration to an Aerodynamic Gust Load.

While the frequency domain response is informative on how the different structural modes interact with a gust, most engineers are interested in the real, time-domain response of a configuration and how that relates to stresses on the configuration. Figure 3 shows the time domain vertical displacement and Von Mises stress response of the configuration to a gust. As is expected the maximum stress corresponds to the maximum displacement of the tip nodes but for the 6 inch panel, there is potential weight savings for configuration as the Von Mises stress constraints are not active.

Distribution Statement A: Approved for Public Release; Distribution is Unlimited. PA# AFRL-2024-2907.

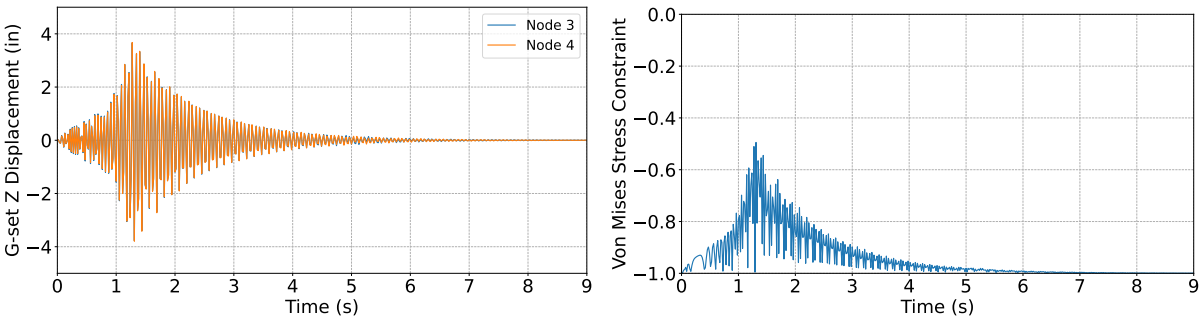

(a) Vertical Displacement of Tip Nodes in Time. (b) Panel Von Mises Stress in Time.

Figure 3: Time-Domain Gust Responses for 6 inch Panel Design.

The results in Figure 4 shows how each optimization performed, with both problems able to satisfy the tolerances on constraint satisfaction. Both optimization problems resulted in similar final designs, but the analytical sensitivities were able to converge to a local design quicker than the finite difference approximations. Overall the optimizer was able to use stress sensitivities of mass and Von Mises stress constraints to reduce the mass of the configuration by 25% while also satisfying the strength constraints for both problems. The final design of the analytical optimization was a 4.2878 inch thick panel where as the finite difference approach resulted in a 4.2829 inch thick panel. Differences in the final design while small are attributed to errors in the analytical sensitivity calculations. A rigorous verification of the analytical sensitivities was not completed, but they appear to be sufficient for simple design problems.

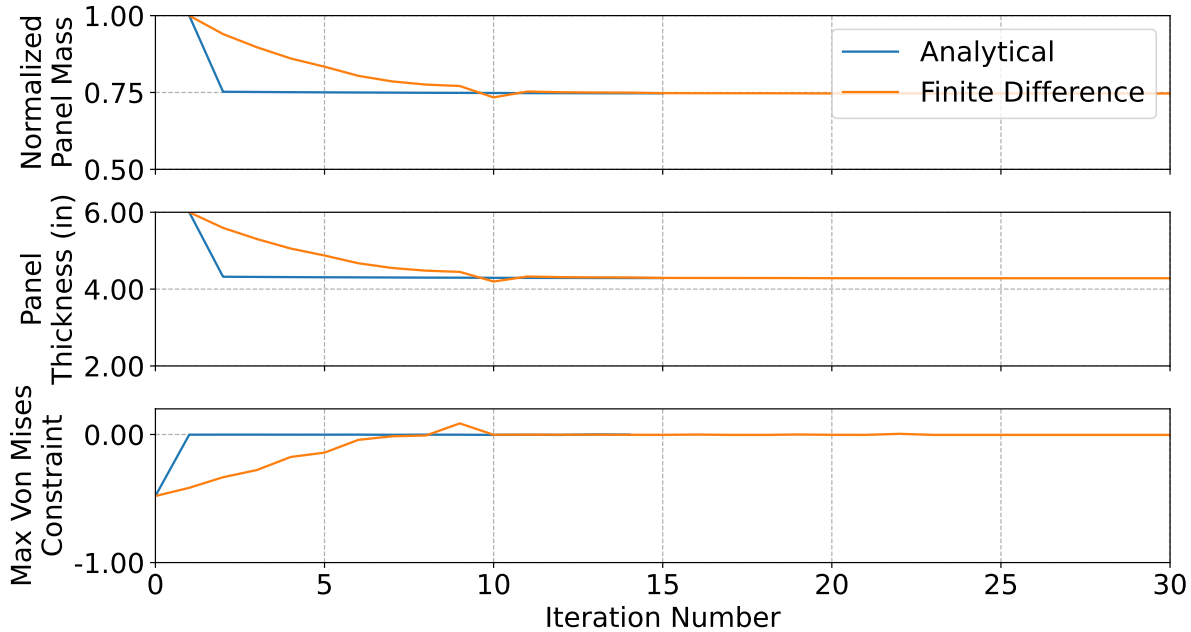

Figure 4: Structural Mode Shapes of Panel Wing Configuration.

Since this is a one-dimensional design problem, the final solution of the optimizations were examined to ensure it was at or near the optimal design as well as an examination of the entire constraint space. Figure 5 shows a contour of the constraint values for the range of solution times as well as a range of panel thickness values. This shows the 'hot-spots' of the design space where the Von Mises stress constraints will become active. The optimization trajectories for both problems are shown to ensure that the optimizer is not taking a path towards a locally

Distribution Statement A: Approved for Public Release; Distribution is Unlimited. PA# AFRL-2024-2907.

minimum solution. At the final design point for the analytical optimization problem there is further room for mass minimization as the Von Mises constraints are not fully active. It is likely the optimizer was unable to find a new search direction which remained feasible at the final design due to noisy analytical constraint gradients. The finite difference optimization was able to push the design closer to the constraint boundary due to its smoother gradients.

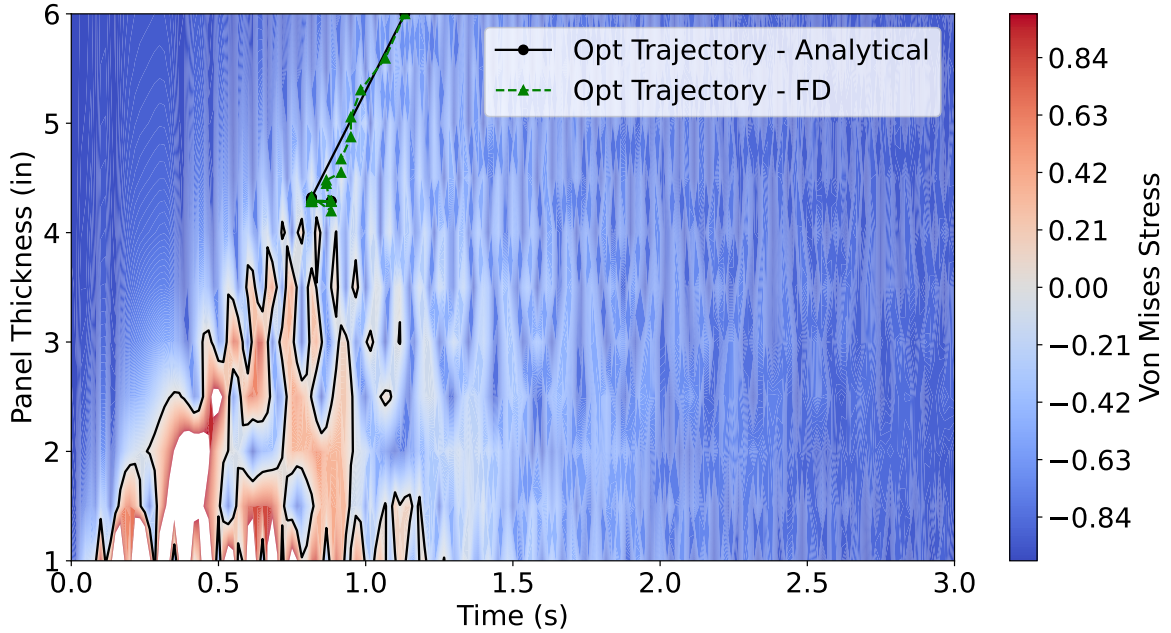

Figure 5: Structural Mode Shapes of Panel Wing Configuration.

Figure 7 shows the modal response of the final design which exhibits similar characteristics to that of the initial design. The response of the bending mode has greatly increased and the harmonic response of the torsion mode also appears to have increased. Like the initial design, the natural frequencies of the panel correspond to the greatest amplitude of the modal response to a gust. Figure 6 shows that the maximum displacement has increased from approximately 4 inches to nearly 10 inches and the Von Mises stress response shows that the constraints are nearly active at the maximum displacement. It is important to note that for the panel design, the tip displacement still remains less than 10% of the total span, even for a more compliant panel design. The natural frequencies of the elastic modes have decreased to 6.40 Hz and 28.30 for bending and torsion respectively.

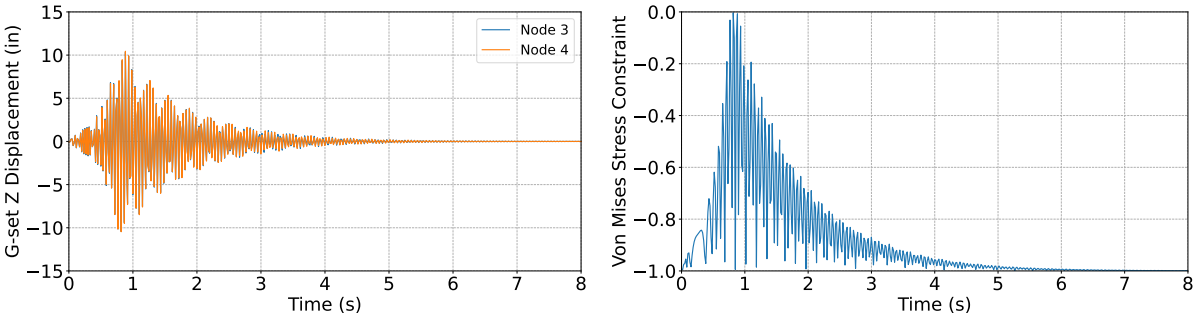

(a) Vertical Displacement of Tip Nodes in Time.

(b) Panel Von Mises Stress in Time.

Figure 6: Time-Domain Gust Responses for 4.2829 inch Panel Design.

Distribution Statement A: Approved for Public Release; Distribution is Unlimited. PA# AFRL-2024-2907.

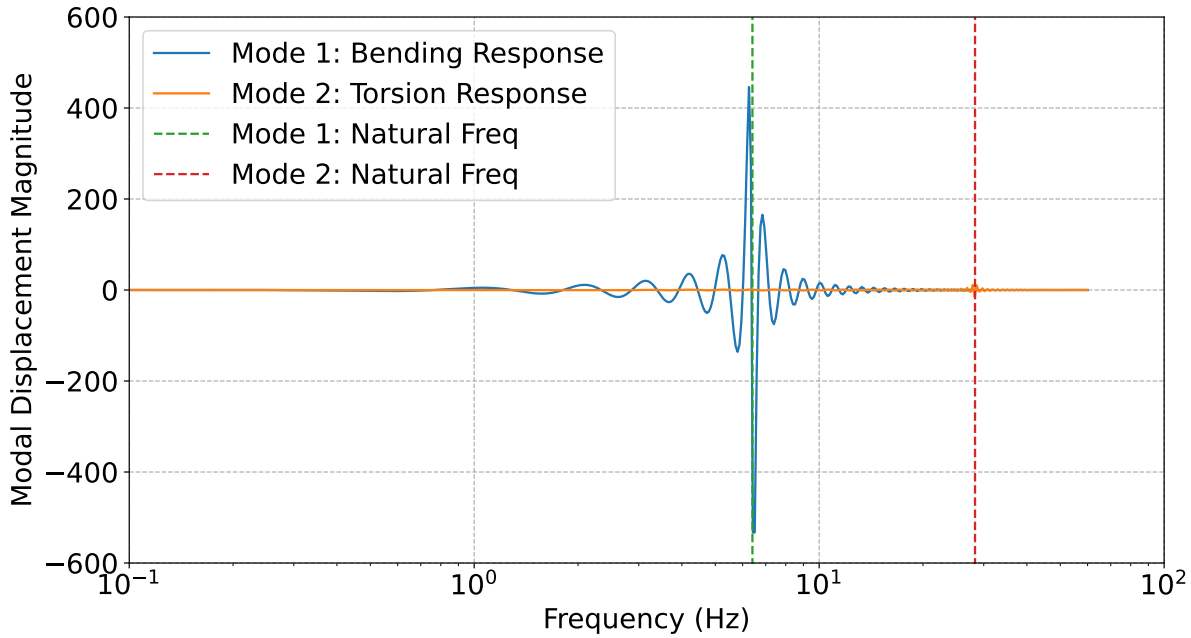

Figure 7: Modal Response of a Panel Wing Configuration to an Aerodynamic Gust Load.

5 CONCLUSIONS

The research performed is an initial step at including aeroelastic stress constraints from gust analysis within a gradient based optimization. Efforts to integrate directly with ASTROS were limited in success, however it was demonstrated that inclusion of external optimization tools yields a viable solution. The gradient-based optimization was successfully able to reduce the mass of the wing panel configuration while maintaining a feasible structural design for both the analytical and finite difference gradient approximations. Examination of the design constraint space shows that the optimizer was able to successfully find the near minimum solution and the behavior of the design space is encouraging for design problems with increasing number of design variables. Due to the nature of how ASTROS's optimizer the modified method of feasible directions works, it is encouraging that the overhead of additional constraints will be limited with the handling of an 'active-set'. This will limit the number of sensitivity calculations for the constraints and enables the use of 'approximate problem' optimization techniques. Future work is planned to verify the analytical sensitivity equation as well as increase the number of design variables and incorporate representative gust loads for certification. The hope is to incorporate these changes into ASTROS, but external verification and development will be leveraged if required.

6 REFERENCES

[1] Andrew S Thelen, Dean E Bryson, Bret K Stanford, and Philip S Beran. Multi-fidelity gradient-based optimization for high-dimensional aeroelastic configurations. *Algorithms*, 15(4):131, 2022.

[2] Bret Stanford. Aeroservoelastic optimization under stochastic gust constraints. In *2018 Applied Aerodynamics Conference*, page 2837, 2018.

[3] E Livne, LA Schmit, and PP Friedmann. Integrated structure/control/aerodynamic synthesis of actively controlled composite wings. *Journal of Aircraft*, 30(3):387–394, 1993.

[4] Andrew S Thelen, Bret Stanford, and Kevin Jacobson. Flutter and stochastic gust constraint studies of the undeflected crm using mphys. In *AIAA Scitech 2024 Forum*, page 2774, 2024.

Distribution Statement A: Approved for Public Release; Distribution is Unlimited. PA# AFRL-2024-2907.

[5] DJ Neill, DL Herendeen, and VB Venkayya. Astros enhancements, volume 3: Astros theoretical manual. Technical report, WL-TR-93-3006, 1995.

[6] James E. Kinnu John M. Griffin. B-2 systems engineering case study. Technical report, Air Force Center for Systems Engineering, Air Force Institute of Technology, 2007.

[7] Robert T Britt, Steven B Jacobson, and Thomas D Arthurs. Aeroservoelastic analysis of the b-2 bomber. *Journal of Aircraft*, 37(5):745–752, 2000.

[8] Justin S. Gray, John T. Hwang, Joaquim R. R. A. Martins, Kenneth T. Moore, and Bret A. Naylor. OpenMDAO: An open-source framework for multidisciplinary design, analysis, and optimization. *Structural and Multidisciplinary Optimization*, 59(4):1075–1104, April 2019.

Distribution Statement A: Approved for Public Release; Distribution is Unlimited. PA# AFRL-2024-2907.